ATP burst is the dominant driver of antibiotic lethality in Mycobacteria

Tejan Lodhiya[1], Aseem Palande[1], Anjali Veeram[1], Gerald Larrouy-Maumus[2], Dany J V Beste[3], Raju Mukherjee[*1]

[1]Department of Biology, Indian Institute of Science Education and Research (IISER), Tirupati, India
[2]MRC Centre for Molecular Bacteriology and Infection, Department of Life Sciences, Faculty of Natural Sciences, Imperial College London, London, UK
[3] Department of Microbial Sciences, Faculty of Health and Medical Sciences, University of Surrey, Guildford, UK
*Corresponding author - raju.mukherjee@iisertirupati.ac.in

Abstract: Antibiotic-tolerant bacteria, due to their unique physiology, are refractory to antimicrobial killing and pose challenges for successful therapy. *M. tuberculosis*, the causative agent of tuberculosis (TB), is exceptionally difficult to control due to antibiotic tolerance. Incomplete knowledge of how bactericidal antibiotics work has impeded our understanding of the development of antibiotic tolerance in mycobacteria. In this study, using quantitative proteomics, ^{13}C-isotopomer analysis, and biochemical assays, we investigated the physiological response of *M. smegmatis* challenged with sub-lethal doses of aminoglycoside and fluoroquinolone antibiotics. Two distinct classes of antibiotics elicited remarkably similar bacterial responses in central dogma, cell division, and central carbon metabolic processes. Both antibiotics increased TCA cycle flux, resulting in enhanced respiration, reactive oxygen species (ROS) production, and ATP burst. While both ROS and ATP burst were found to contribute to antibiotic lethality, our findings indicate that ATP burst, and not ROS, is the dominant cause of antibiotic-induced cell death in mycobacteria. ^{13}C isotope tracing experiments indicated metabolic bifurcation of the TCA cycle flux from the oxidative arm into glutamate-glutamine-GABA as a potential bacterial adaptive mechanism to reduce the production of reactive oxygen species (ROS) and ATP burst. In addition, antibiotic-adapted mycobacteria have an activated intrinsic drug resistance mechanism, a higher mutation rate, and are prone to developing antibiotic resistance. Our study provides a novel understanding of the intricate mechanisms of antibiotic-induced cell death, and has significance for the design of combinatorial interventions and adjuvant therapy against one of the most successful infectious diseases.

Introduction: Antibiotics have saved millions of lives from bacterial infections, including those caused by Mycobacterium, Pseudomonas, and Staphylococcus, among others. However, the emergence of antimicrobial resistance (AMR) against all classes of antibiotics renders clinically available antibiotics ineffective and undermines efforts to combat lethal bacterial pathogens. Antimicrobial resistance (AMR) is presently responsible for approximately 7,00,000 deaths per year, and if left unchecked, this number is projected to exceed 10 million by 2050 (1). The conventional technique for combating AMR has been the production of novel pathogen-specific antibiotics; however, this is no longer a viable option, as the drug discovery pipeline has not produced any new classes of antibiotics over the past several decades. Consequently, there is a pressing need to develop novel methods for preserving and enhancing the efficacy of existing drugs through drug synergism or adjuvant therapy. However, there are gaps in our understanding of how precisely existing antibiotics mediate cell death and what are bacterial counter responses to these challenges at the system-wide scale.

It was previously believed that antibiotics kill bacteria by compromising essential cellular processes such as DNA replication, transcription, and translation. Consequently, resistance mechanisms include target mutations, the presence of antibiotic-inactivating enzymes, antibiotic efflux, etc. Interestingly, in 2007, Kohanski *et al.* proposed that distinct antibiotics have a common mode of action through the production of reactive oxygen species (ROS), regardless of the target(2). Subsequently, respiration-decelerating antibiotics were found to inhibit the bactericidal activity of respiration-accelerating antibiotics(3), highlighting the significance of an in-depth understanding of the drug's mode-of-action, particularly for combinatorial treatment. While the deleterious effect of ROS on bacterial physiology is expected, at sub-lethal concentrations, these reactive oxygen species can promote multidrug resistance by inducing superoxide radical-induced mutations(4). These observations demonstrate that the mechanism of antibiotic lethality is more complicated than previously understood. Therefore, it is crucial to look beyond drug-target interactions and comprehend the numerous mechanisms by which antibiotics induce cell death. The bacterial counter responses to these mechanisms could result in the emergence of antibiotic tolerance and, eventually, resistance.

Antibiotic tolerance is the result of physiological adaptation that enables bacteria to withstand lethal antibiotic doses for longer periods of time, and this population has the potential to become genetically resistant to antibiotics(5). Although the significance of antibiotic tolerance is recognized, the precise metabolic state and sequence of adaptive events leading to the development of antibiotic tolerance remain poorly understood. *M. tuberculosis (Mtb)*, the etiological agent for tuberculosis, which remains a prominent cause of death worldwide (1.5 million per year), is exceptionally tolerant to antibiotics and it is thought to explain why the treatment for tuberculosis requires a combination of antibiotics administered for at least six months (6). The rapid increase in multi- and extensively drug-resistant tuberculosis (MDR & XDR-TB) infections, which is facilitated by antibiotic tolerance, compels us to re-examine our current understanding of the mechanisms of antibiotic action in mycobacteria and bacterial responses to antibiotic exposure.

Therefore, the systematic investigation of the bacterial physiological responses to antibiotic exposure prior to the emergence of drug resistance holds the key to deciphering the nature and magnitude of the antibiotic-induced stresses and subsequently increasing our understanding of the mechanisms of antibiotic tolerance preceding resistance. In this study, we employed temporal quantitative proteomics and ^{13}C isotopomer analysis to comprehensively understand the physiological responses of the model organism, *M. smegmatis* (Msm), exposed to sub-lethal concentrations of two classes of bactericidal antibiotics, fluoroquinolone and aminoglycoside. Further biochemical and microbiological tests showed the involvement of ROS and ATP burst in antibiotic lethality, with ATP burst being the dominant factor driving cell death. Our findings contribute to a deeper understanding of the complex mechanisms underpinning antibiotic-induced cell death in mycobacterium and have implications for preventing the development of antibiotic tolerance and resistance.

Results:

Exposure to sub-lethal doses of aminoglycoside and fluroquinolone reveals physiological adaptation without antibiotic resistance

To better understand the biology of antibiotic-stressed mycobacteria, we designed a growth assay to measure the responses of mycobacteria to sublethal antibiotic concentrations. Wild-type *M. smegmatis mc²155* was challenged with either 1x, ½x, or ¼x MBC_{99} (minimum bactericidal concentration) of fluoroquinolone (norfloxacin) and aminoglycoside (streptomycin) antibiotics. While 1x MBC_{99} and ½x MBC_{99} concentrations were lethal and growth-inhibitory, respectively, growth at sub-lethal concentrations (i.e., ¼x MBC_{99}) of both antibiotics exhibited a prolonged lag phase **(Fig. 1A and 1B)**.

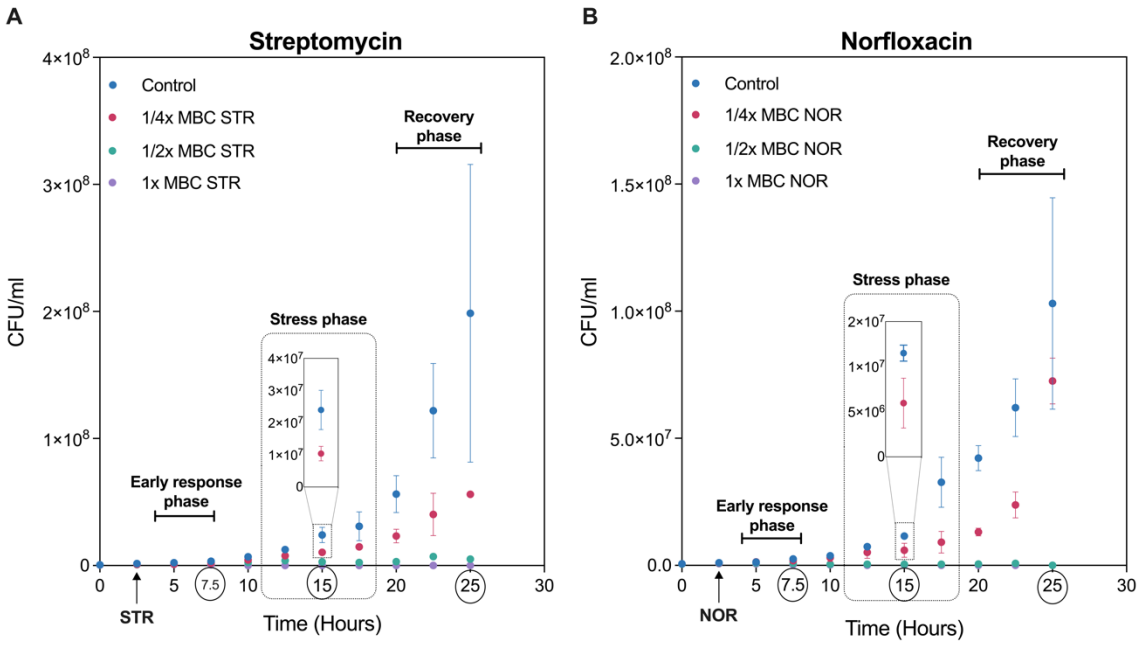

Fig. 1. Exposure to sub-lethal doses of aminoglycoside and fluroquinolone reveals physiological adaptation to antibiotics.

The growth curve of *M. smegmatis* challenged with either 1x, ½x, or ¼x MBC_{99} of streptomycin (A) or with norfloxacin (B). Data points represent the mean of at least three independent replicates ± SD. 1x MBC_{99} of streptomycin (250 ng/ml) and 1x MBC_{99} of norfloxacin (2 µg/ml).

To better understand the antibiotic-induced growth changes, we divided the growth curve into three phases: an early response phase (t =7.5 hours, 5 hours post antibiotic treatment), which is a period shortly after the addition of antibiotics, showing no visible differences in the growth rate; a stress phase (t = 15 hours, 12.5 hours post antibiotic treatment), characterized by reduced growth rate and prolonged lag time; and a recovery phase (t =25 hours, 22.5 hours post antibiotic treatment), in which mycobacterial growth rate resumes following antibiotic adaptation. The experiments were terminated when the culture reached stationery phase (~ OD = 1) to prevent the stationery phase response from interfering with the antibiotic response. The

prolonged lag time observed during the stress phase is of profound significance in deciphering the nature of antibiotic-induced stresses and has implications for the development of antibiotic tolerance(7). Similarly, a thorough understanding of the recovery phase cells can reveal cellular determinants involved in antibiotic adaptation. Towards this end, we first ruled out whether the resumption of growth on sub-lethal concentrations of antibiotics was due to the emergence of an antibiotic-resistant population. For this, bacteria were harvested from the recovery phase (25-hour point) and the MICs of cells grown with and without ¼x MBC_{99} of antibiotics were compared. No changes in the MICs confirmed that the growth resumption during the recovery phase was physiological rather than a result of the development of antibiotic resistance **(S1A and S1B)**.

Norfloxacin and Streptomycin have common mechanism of action

To deduce the physiological alterations in mycobacterium exposed to antibiotics, untargeted label-free quantitative (LFQ) proteomics was performed on mycobacteria grown with and without ¼x MBC_{99} of both antibiotics during all three growth phases. All six data sets yielded a total of 2,982 distinct protein groups (43% of the *M. smegmatis* proteome), with each sample identifying roughly 2000 proteins **(S2A)** demonstrating the robustness of our methodology. To ascertain the reproducibility of data across samples **(S2B)**, the data for each condition were subjected to rigorous quality control analysis. Differentially expressed proteins were defined as those with a fold change threshold of ±2 and a t-test significance cut-off of ≤ 0.05. The volcano plot analysis revealed the differential expression of several proteins in response to both antibiotics **(Fig. 2A and 2B)**.

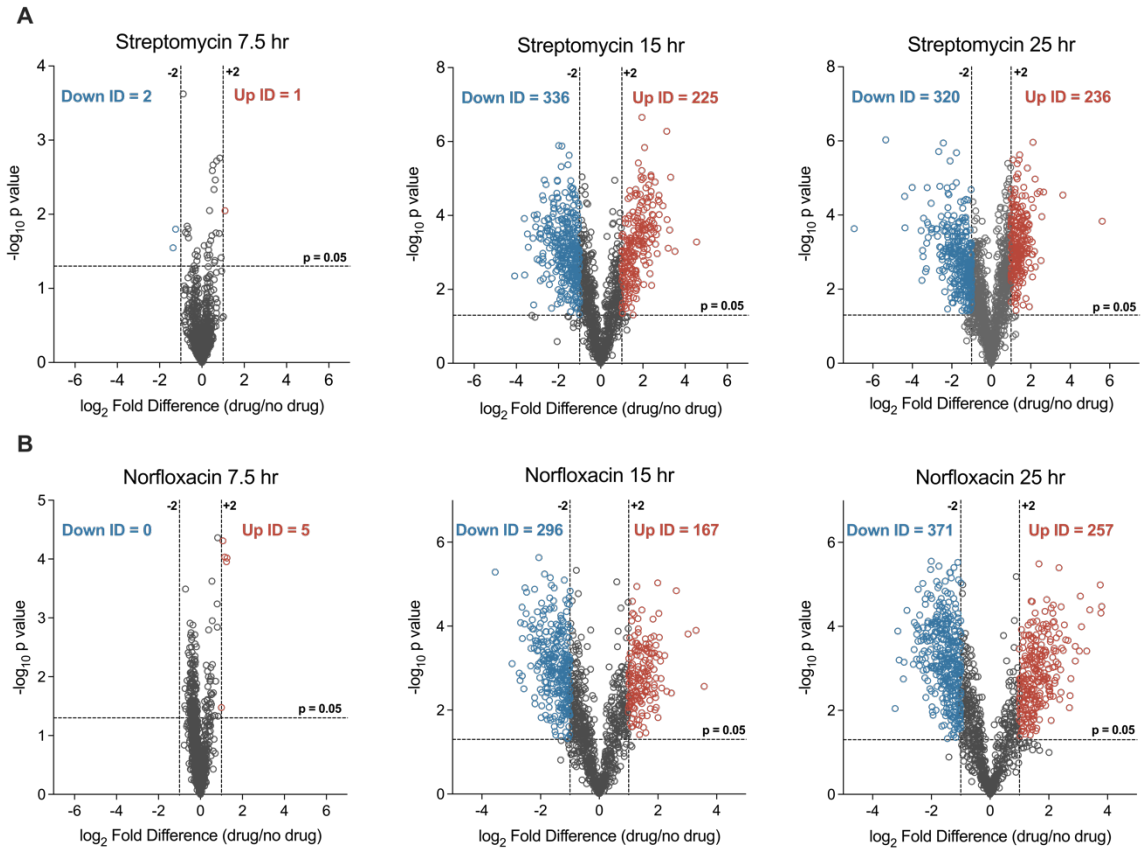

Fig. 2. Differential expression analysis of proteome upon norfloxacin and streptomycin treatment

Volcano plot analysis of the proteins temporally quantified at 7.5 hr, 15 hr, and 25 hr time points for streptomycin (A) norfloxacin treatment (B). Each dot represents one protein. Fold change cut off ±2 and a t-test significance cut-off of ≤ 0.05 were applied to identify differentially expressed proteins, shown in different colors.

Corresponding to the fact that the growth rate of cells in the early response phase (7.5-hour) was unaffected, the proteomic profile of antibiotic-treated cells was undistinguishable from that of the control group at time point. In contrast, cells from the stress phase (15-hour) and the recovery phase (25-hour) displayed a number of up- and down-regulated proteins in response to both the antibiotics. Consistent with its mode of action, streptomycin treatment up-regulated proteases, peptidases, and proteasomal complex components implicated in the degradation of misfolded proteins **(Fig. 3A)**. Likewise, norfloxacin treatment induced the SOS response by down-regulating LexA, the repressor of SOS response, and up-regulating DNA repair proteins such as RecA, RecB, RecC, and PafC **(Fig. 3A)**. These data indicate that the sub-lethal doses of antibiotics used in our study exert sufficient stress on their primary targets. Next, we sought to determine the secondary consequences of antibiotic-target interactions. Towards this end, proteins involved in central dogma (DNA replication, transcription, and translation), and cell cycle and cell division processes were significantly down-regulated in response to both the antibiotics **(Fig. 3B to 2D)**, correlating with the observed decrease in growth rate during the stress phase. Our results suggest that the initial bacterial response to antibiotics may be the downregulation of essential cellular processes that are required for optimal growth and antibiotic lethality.

To look for common modes of antibiotic action as have been previously reported in *E. coli*(2,8), we performed a Pearson correlation analysis between the norfloxacin and streptomycin induced proteome from the stress phase **(Fig. 3E)** and recovery phases **(S3A)** of our assay. This analysis revealed a highly correlated (Pearson coefficient (r) > 0.90) proteomic profile of antibiotic-treated mycobacteria in stress phase **(Fig. 3E)**, indicating that structurally and functionally distinct antibiotics produce a strikingly similar proteomic response. To determine the cause of these similarities, we attempted to gain a deeper understanding of the processes commonly impacted by antibiotics. For this, we conducted pathway enrichment analysis on proteins that were up-regulated as well as exclusively expressed upon antibiotic treatments. As depicted in **(S3B)**, pathway enrichment analysis showed that central carbon metabolic pathways were enriched for both the antibiotics. Notably, enzymes of TCA cycle (CitA, Icd, Acn), glyoxylate shunt (Icl1 and GlcB), GABA shunt, and the anaplerotic node (Pck, Pca) were significantly up-regulated for both antibiotics, suggesting metabolic alterations in response to antibiotic treatment (**Fig. 3F and 3G)**. Collectively, these data advocate for a common mechanism of antibiotic action that extends beyond their primary targets.

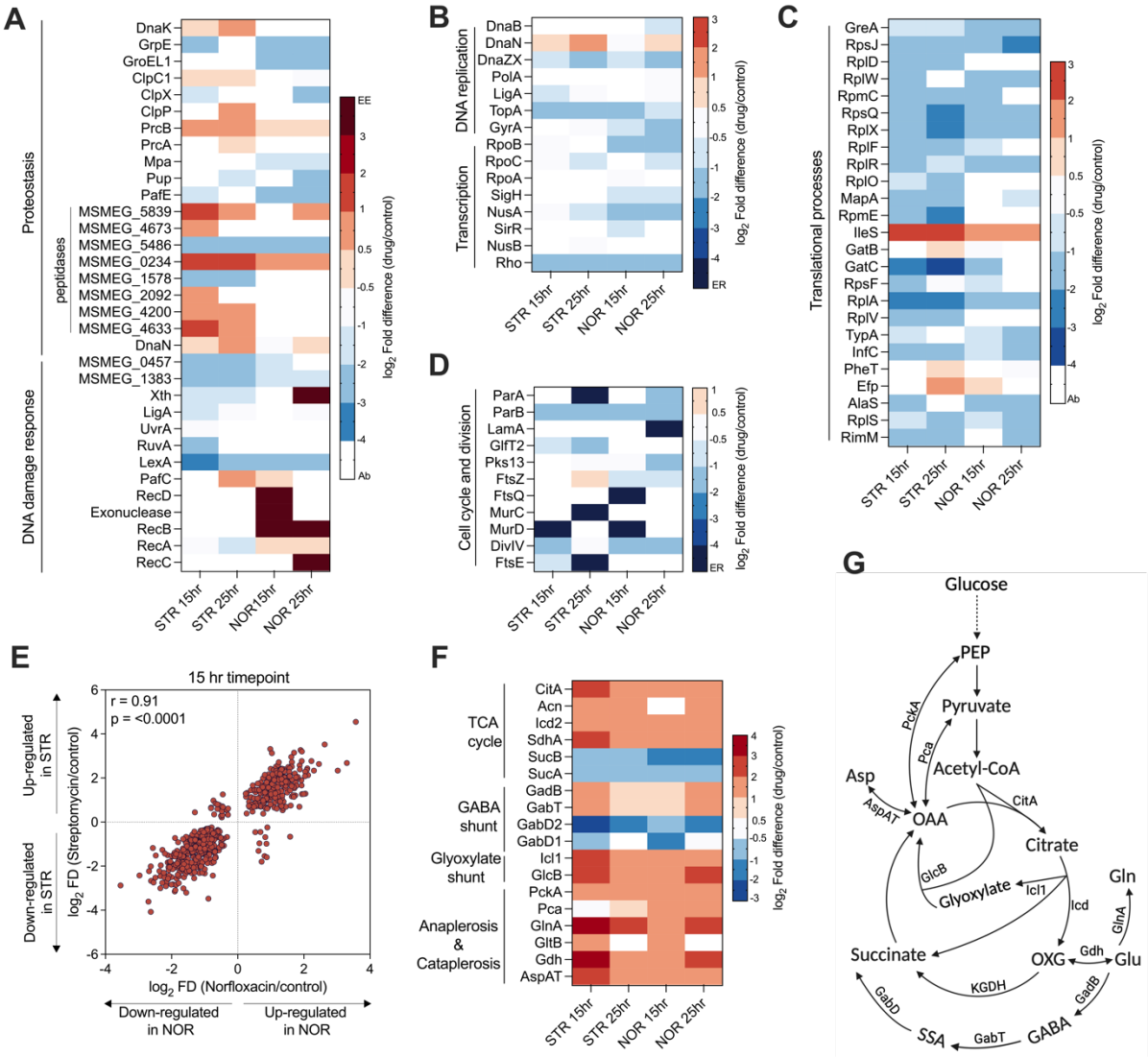

Fig. 3. Norfloxacin and Streptomycin have common mechanism of action

Heat map analysis represents the $\log_2$ fold changes of proteins involved in (A) DNA damage response and proteostasis network, (B) DNA replication and transcription, (C) translation, and (D) cell cycle and cell division processes, identified from proteomics data. Colours in the heat map depicts the extent of differential expression, where EE demonstrates exclusively expressed, ER demonstrates exclusively repressed/absent in response to antibiotics, and Ab represents proteins that were not identified or quantified with high significance. (E) Scatter plot depicting the Pearson correlation analysis of common proteins identified in norfloxacin and streptomycin treatment. Each dot represents a single protein with its $\log_2$ fold difference for NOR (x-axis) and STR (y-axis) treatment at t = 15 hour time point. (F) Heat map depicting the $\log_2$ fold changes of proteins involved in central carbon metabolism (CCM) of *M. smegmatis*. Figure (G) illustrates the CCM pathway of *M. smegmatis*.

Norfloxacin and Streptomycin generate reactive oxygen species (ROS) as part of their lethality

It is hypothesized that reactive oxygen species (ROS) are generated as a secondary consequence of antibiotic-target interaction and facilitate antibiotic-induced cell death by oxidizing vital biomolecules(7). We hypothesized that bacteria treated with antibiotics would

induce the antioxidant response if antibiotics generate ROS. In accordance with this hypothesis, proteomics data mining revealed a significant upregulation of anti-oxidant enzymes such as catalases, superoxide dismutases, mycothione reductase, and methionine sulfoxide reductase (MsrA) (**Fig-4A)**. The upregulation of enzyme MsrA, involved in the repair of the oxidized proteins, indicates ROS mediated protein oxidation. In addition, anti-oxidant proteins such as alkylhydroxyperoxidase, bromoperoxidase, and peroxiredoxin were exclusively expressed in response to antibiotics, suggesting that bacteria may have experienced oxidative stress upon antibiotic treatment. Together, these data suggest that the treatment of NOR and STR induces reactive oxygen species (ROS) production.

To directly measure oxidative stress (due to intracellular ROS production) in response to antibiotics, we used the Mrx1-roGFP2 redox biosensor(9). It is a ratio-metric fluorescence reporter that measures the redox potential of mycobacteria and has been extensively used to measure the redox state of cells *in-vitro* and *ex-vivo* (9–11). The sensor exhibits an increased ratio of fluorescence at 405/488 nm under oxidative stress, and a reduced ratio under reductive stress. The ability of the biosensor to measure oxidative and reductive stress was confirmed using the oxidizing agent (menadione) and the reducing agent (GSH). As anticipated, treatment with menadione increased the fluorescence ratio at 405/488 nm, while treatment with GSH decreased the fluorescence ratio in comparison to the untreated control **(S4A)**, demonstrating the feasibility and reliability of this biosensor in detecting oxidative stress in mycobacteria.

Next, to interrogate whether the antibiotics induce ROS production and oxidative stress, we administered sub-lethal to lethal doses of both antibiotics to a biosensor containing bacteria. The exposure to either NOR or STR increased the ratio of fluorescence at 405/488 nm, showing that antibiotics induce ROS in a time **(Fig. 4B and 4C)** and concentration-dependent manner **(Fig. 4D and 4G)**. Next, we sought to investigate whether ROS contributed to antibiotic lethality. Towards this end, we first established whether glutathione (GSH) can quench antibiotic-induced ROS. The co-treatment with GSH prevented an increase in the 405/488 nm ratio upon antibiotic treatment **(S4B and S4C)**. Next, to understand the impact of ROS on cell survival, an antibiotic time kill curve was performed with a supra-lethal dose (10x-MBC_{99}) of antibiotics over a duration predetermined to result in the death of > 99.9% of cells(12), with and without GSH. As depicted in (**Fig. 4E and 4H)**, the co-administration of GSH substantially inhibited the lethality of antibiotics, demonstrating that antibiotic-induced ROS contributes to cell death.

It is known that ROS damages nearly all biomolecules, including DNA, proteins, and lipids. Proteins of TCA cycle enzymes and the ETC chain harbour Fe-S clusters for electron exchange that are very susceptible to ROS-induced damages, resulting in the release of iron (Fe^{+2}) in the cytoplasm. Free hydroxyl radicals are generated via the Fenton cycle, which results in further ROS production and could also contribute to antibiotic-induced cell death(13). Using the iron-chelator bipyridyl (BP), known to inhibit the Fenton cycle-mediated ROS burst, we found that indeed iron chelation significantly reduced antibiotic induced-death **(Fig. 4F and 4I)**. Collectively, the induction of the antioxidant response, the detection of ROS using the Mrx1-roGFP2 biosensor, and the mitigation of antibiotic lethality using glutathione and Fenton cycle inhibitor show that both NOR and STR treatment cause increased ROS production, which plays

a crucial role in antibiotic lethality.

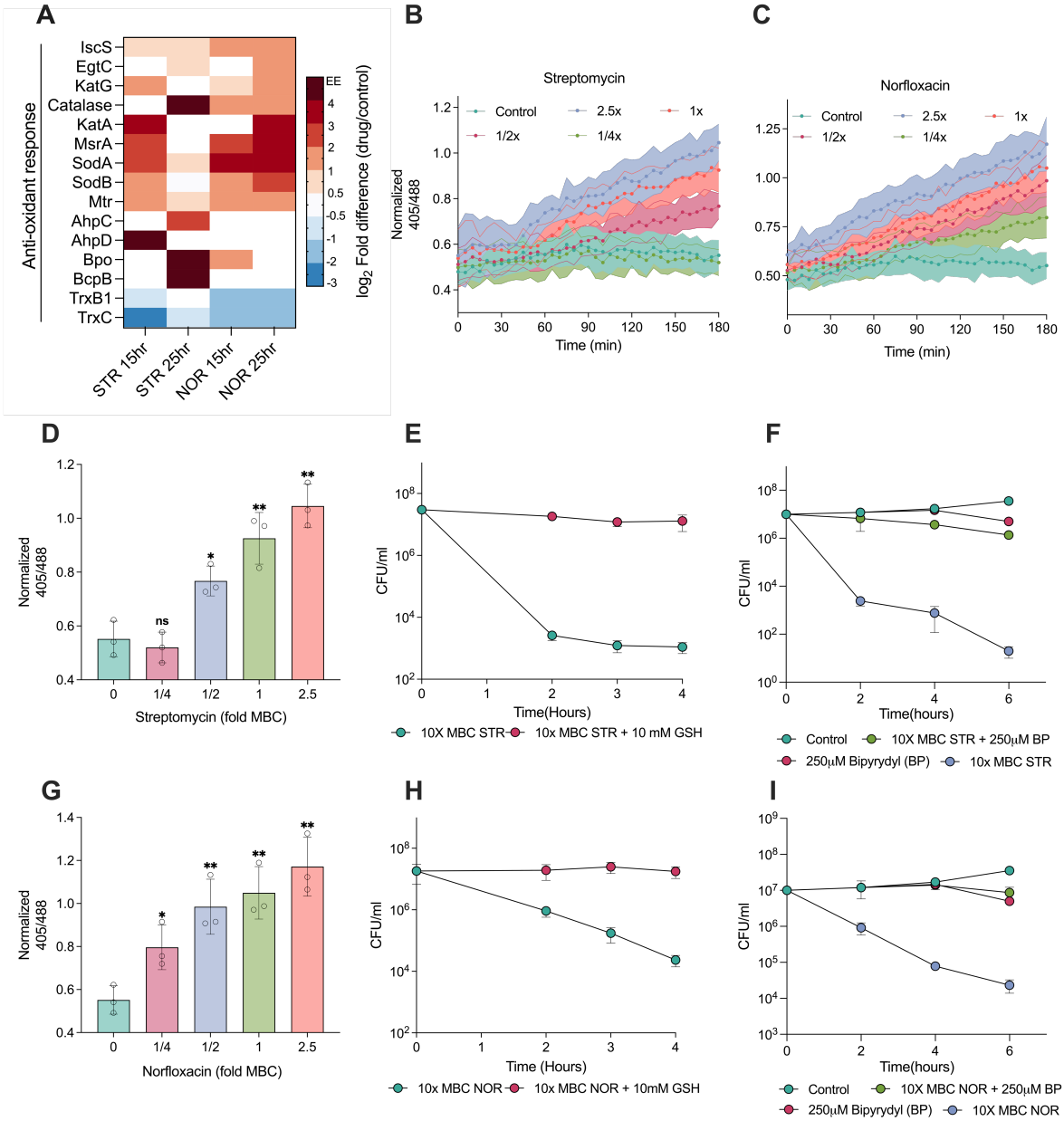

Fig. 4. Norfloxacin and Streptomycin generate Reactive oxygen species (ROS) as part of their lethality

The heat map (A) depicts the $\log_2$ fold differences of proteins involved in antioxidant response. EE demonstrates proteins that are exclusively expressed in response to NOR or STR. Temporal (B and C) and dose-dependent (D and G) ratio metric response of *M. smegmatis* expressing Mrx1-roGFP2 redox biosensor upon streptomycin and norfloxacin treatment at 3 hour. The biosensor fluorescence measurements were recorded at the excitation of 405 nm and 488 nm, for a common emission at 520 nm. Figures demonstrate the effect of 10 mM glutathione on the survival of *M. smegmatis* treated with lethal dose (10x MBC_{99}) of streptomycin (E) and norfloxacin (H). Figures (F) and (I) depict the effect of bipyridyl on the survival of *M. smegmatis* treated with lethal dose of streptomycin and norfloxacin, respectively. Data points represent the mean of at least three independent replicates ± SD. Statistical significance was calculated by students' t-test (unpaired), *$p < 0.05$, **$p < 0.01$, ***$p < 0.001$.

Norfloxacin and Streptomycin treatment induces a burst in ATP levels

Despite knowing the significance of ROS, the precise cause, stimulus and its origin remain poorly understood. Since the electron transport chain (ETC) is the primary source of electron leakage and ROS production, we hypothesized that the increase in ROS production was the result of enhanced respiration. To explicitly test this, we measured the levels of ATP, the final product of aerobic respiration, in response to antibiotics. As depicted in **(Fig. 5A to 5F)**, NOR and STR treatments induced a time- and dose-dependent increase in ATP production, suggesting an increase in respiration. The increased respiration was also confirmed using the redox dye resazurin as reported earlier (14). As depicted in **(S5A to S5F),** resazurin assay showed enhanced fluorescence conversion rate in bacteria treated with antibiotics confirming increased respiration rate. Intriguingly, the observed ATP burst under antibiotic treatment was inversely proportional to cell survival, indicating that ATP burst may contribute to mycobacterial death **(Fig. 5A to 5F)**. Notably, the respiration rate has been linked to antibiotic action with accelerated respiration potentiating antibiotic lethality (15). Collectively, our data show that antibiotic-treated cells exhibit significant increase in respiration, resulting in an ATP burst that is associated with cell death.

We next sought to distinguish whether the ATP burst was a consequence or a cause of antibiotic lethality. To establish the role of ATP burst in antibiotic action, a specific inhibition of antibiotic-induced ATP burst without causing a decrease in metabolic rate was required. Towards this, we cotreated cells with antibiotics and carbonyl cyanide 3-chlorophenylhydrazone (CCCP), a protonophore, at non-toxic levels **(S5K)** to mitigate ATP burst. Protonophore uncouples oxidative phosphorylation from ETC, thus relieving the back-pressure on ETC resulting in an increase in respiration. As depicted in **(Fig. 5G, 5H, 5J, and 5K)**, the co-treatment with CCCP dissipated the antibiotic-induced ATP burst in a dose-dependent manner, confirming that the increase in ATP levels mediated by NOR and STR treatment was the result of increased respiration and oxidative phosphorylation. Subsequently, we reasoned that if ATP burst contributes directly to antibiotic action, then dissipating antibiotic-induced ATP burst would increase bacterial survival on antibiotics. To test this hypothesis, we compared antibiotic kill curves with CCCP (mitigating ATP burst) and without CCCP (causing ATP burst). As demonstrated in **(Fig. 5I and 5L)**, the co-treatment with CCCP significantly inhibited antibiotic-induced cell death, demonstrating that ATP burst is directly driving the antibiotic lethality.

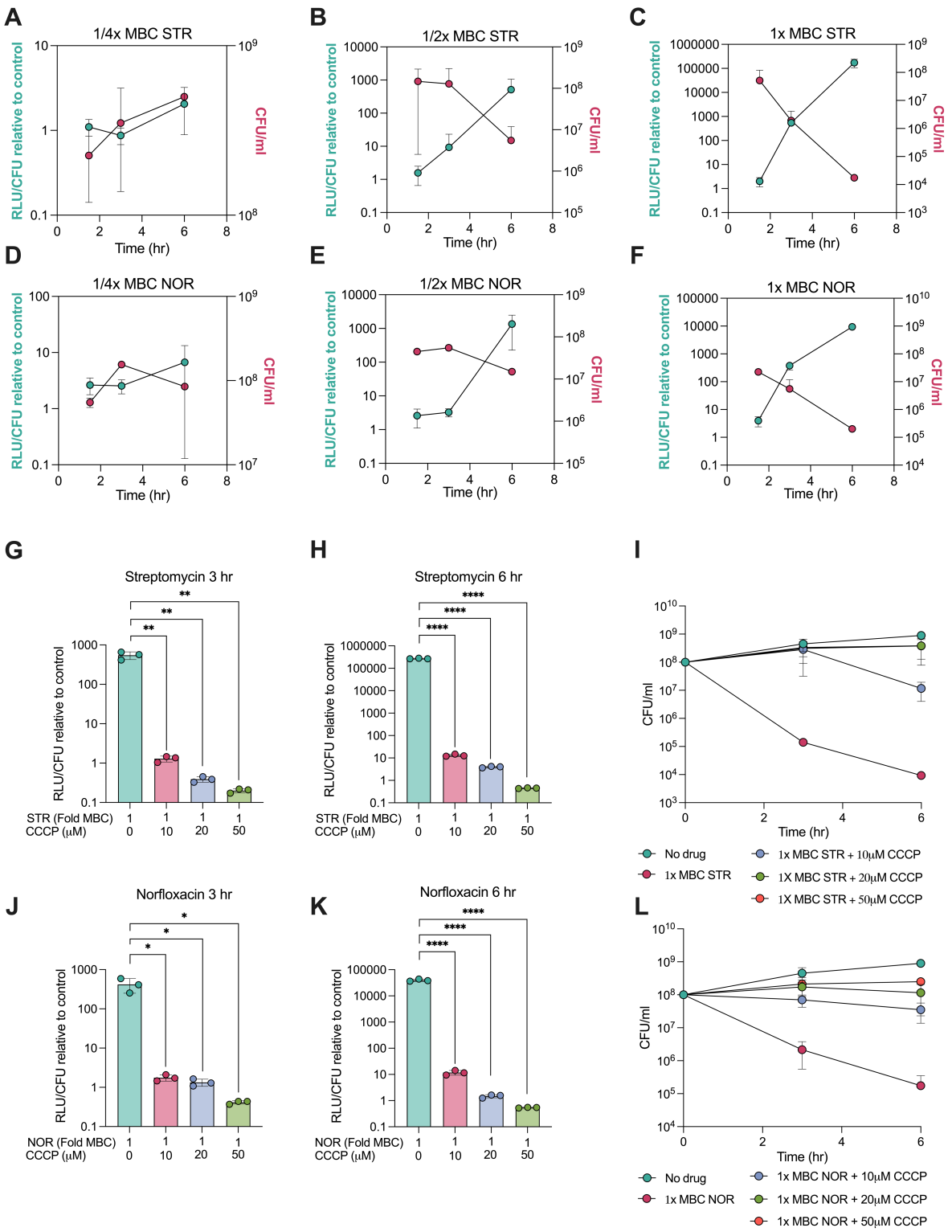

Fig. 5. Norfloxacin and Streptomycin treatment induces a lethal burst in ATP levels

Time-course of relative luminescence measurements representing ATP levels in *M. smegmatis* in response to ¼x (A & D), ½x (B & E) 1x MBC_{99} (C & F) of streptomycin & norfloxacin, respectively. The right y-axis represents the viability of cells measured just before the measurement of ATP. Bar graphs depict the dose-dependent reduction in ATP levels upon CCCP co-treatment with streptomycin (G and H) and norfloxacin (J and K).The effect of increasing concentrations of CCCP on time course survival of *M. smegmatis* challenged with lethal dose of streptomycin (I) and norfloxacin (L), respectively. All data points represent the mean of at least three

independent replicates ± SD. Statistical significance was calculated by students' t-test (unpaired), *p < 0.05, **p < 0.01, ***p < 0.001, ****p < 0.

ATP burst is the dominant driver underpinning antibiotic induced mycobacterial death

Thus far, our data demonstrate that both NOR and STR treatments cause increased ROS generation and ATP burst. After establishing the fact that inhibiting either ROS production or elevated ATP levels can inhibit antibiotic-induced cell death, we sought to determine which of these two mechanisms is the dominant driver of cell death. To determine this, ROS levels were compared under the conditions of ATP burst formation (antibiotic treatment alone) and ATP burst mitigation (antibiotic plus CCCP co-treatment). We reasoned that if ROS is the dominant mechanism driving cell death, then CCCP co-treatment may have also decreased ROS levels to impart enhanced survival in response to antibiotics. As depicted in **(Fig. 6A to 6D)**, the data show that antibiotic treatment alone increased the ratio of fluorescence at 405/488 nm and caused cell death for both the antibiotics. Intriguingly, while the CCCP-mediated inhibition of ATP burst increased cell survival, the 405/488 nm ratio remained higher in surviving cells (increased oxidative stress due to ROS production), indicating that the ATP burst, and not ROS production, is the dominant mechanism driving antibiotic lethality in mycobacteria.

Our results suggest that oxidative stress alone, as mediated by elevated ROS levels, is insufficient to cause cell death. It also points out that ROS is a by-product of antibiotic action (i.e., enhanced respiration) rather than the predominant secondary mediator of cell death, as originally understood. Notably, the CCCP-mediated increase in respiration was also evident from a dose-dependent increase in 405/488 nm ratios with CCCP treatment alone **(S5G and S5H)**. In summary, our results show that NOR and STR treatments increase respiration, resulting in a lethal ATP burst (with ROS generated as a by-product of increased respiration) that mediates mycobacterial death. However, the precise mechanism by which ATP burst mediate cell death remains to be understood.

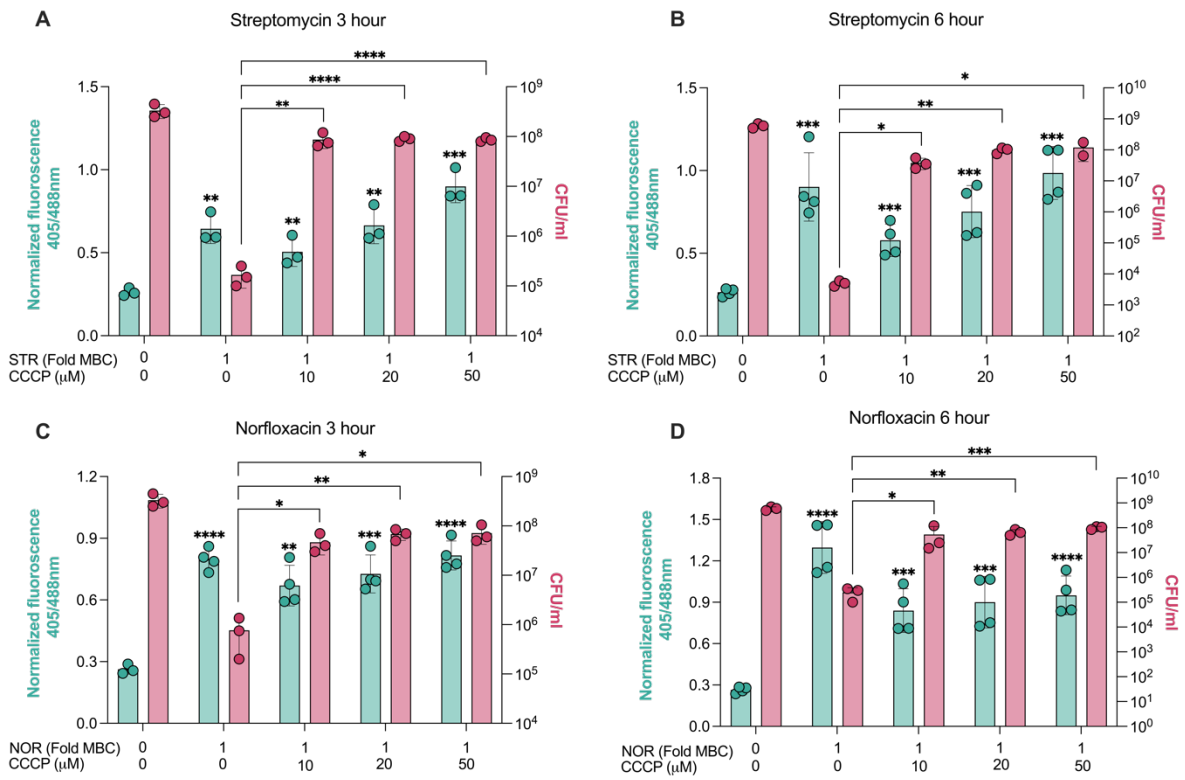

Fig. 6. Norfloxacin and streptomycin induced ROS is insufficient to mediate cell death

Ratio metric response of *M. smegmatis* expressing Mrx1-roGFP2 redox biosensor (left y-axis) and the cell viability (right y-axis) in response to streptomycin (A & B) and norfloxacin (C & D) with and without the co-supplementation with CCCP post 3 hours and 6 hours of treatments. Data points represent the mean of at least three independent replicates ± SD. *p < 0.05, **p < 0.01, ***p < 0.001, ****p < 0.0001 by students' t-test (unpaired).

^{13}C isotopomer analysis suggests increased metabolic flexibility and bifurcation of TCA cycle flux as a bacterial adaptive mechanism

After studying the nature of antibiotic-induced stresses, we sought to investigate bacterial counter responses that could promote antibiotic adaptation and growth recovery. During the recovery phase of our antibiotic assay, ^{13}C isotopologue profiling was performed to investigate the metabolic rewiring underlying growth resumption. Using $^{13}C_6$ glucose as a carbon tracer, the isotopologue profile of intracellular metabolites from central carbon metabolism (at t = 25 hr, treated with ¼x MBC_{99} of NOR or STR) was assessed.

In agreement with the proteomics data, there was an increase in citrate flux **(Fig. 7A)** that correlated with the upregulation of citrate synthase **(Fig. 3F)**. Similarly, there was an increase in flux through the oxidative side of the TCA cycle and towards alpha-ketoglutarate/glutamate production, which correlated with the observed increases in aconitase and isocitrate dehydrogenase levels. The time-dependent increase in the ratio of NADH/NAD+ under NOR and STR treatments **(Fig. 7B)** and a dose-dependent increase for STR treatment **(Fig. 7C)** further confirmed the increased flux measurements through the TCA cycle. The observed increases in the levels of NADH can fuel the ETC chain further to enhance the production of

ATP and generate ROS as a by-product. Collectively, our measurements of increased respiration, ROS production, and ATP production could be explained by an increase in TCA cycle flux following antibiotic treatment.

The decreased flux into pyruvate indicates that phosphoenolpyruvate carboxykinase (PckA), which was upregulated in the proteomic analysis **(Fig. 2F)**, is operating in the anaplerotic direction to fix CO_2 and form oxaloacetate (OAA). It has been demonstrated that the reversal of PEPCK activity is influenced by the redox state of the cells and has been associated with increased ROS production(16). This finding was further corroborated by the increase in aspartate label (a surrogate for oxaloacetate) and M+3 and M+5 ionic species of ^{13}C-citrate **(S6B and S6C)**. This increased flux into OAA can facilitate a greater utilization of acetyl-CoA by the TCA cycle, as indicated by the increased label of citrate.

We exposed bacteria to sub-lethal antibiotic concentrations as our original goal was to provide bacteria with an opportunity to remodel their metabolism and improve their chances of survival. Since antibiotic-mediated death was caused by increased respiration, ATP levels, and ROS, we hypothesized that bacteria at sub-lethal doses may remodel their TCA cycle flux to minimize respiration. In agreement with this hypothesis, the enhanced flux to the oxidative arm of the TCA cycle (to alpha-ketoglutarate/Glu) was found to diverge towards glutamate, glutamine, and GABA shunt following streptomycin treatment **(Fig. 7A)**. This bifurcation of the TCA cycle was facilitated by upregulation of glutamate dehydrogenase, glutamate synthase, glutamine synthetase, and glutamate decarboxylase, as evident from the proteomics data. The amino acids glutamate and glutamine directs the carbon flux from the TCA cycle to amino acid metabolism and play a crucial role in regulating energy and nitrogen metabolism in mycobacteria(17–19). In addition, increased flux in glutamate and GABA would help bypass two enzymatic reactions of the oxidative arm of the TCA cycle and therefore help bacteria restrict the production of reactive oxygen species (ROS) and regulate anaplerosis(20,21). Moreover, we found increased flexibility of the TCA cycle in switching carbon flux from aspartate/ oxaloacetate to alpha-ketoglutarate/glutamate in repones to antibiotics. This reaction is catalyzed by aspartate aminotransferase (AspAT), which was also upregulated in the proteomics data, and has been shown to balance the cataplerosis and anaplerosis of TCA cycle intermediates in mycobacteria(22). Overall, our data suggest that through enhanced expression and activity of TCA cycle enzymes as well as the enzymes of the anaplerotic node (23), the antibiotic-adapted TCA cycle might be more flexible and resilient in terms of minimizing production of ROS and ATP while still maintaining overall metabolism and growth.

The glyoxylate shunt and PPP pathway are involved in antibiotic tolerance mechanisms (24–26). We observed a decrease in the incorporation of ^{13}C label into succinate, indicating a decreased flux through succinate-semialdehyde dehydrogenase (SSADH) or alpha-ketoglutarate dehydrogenase (KGDH) or isocitrate lyase (ICL1). Antibiotic treatments decreased the expression of the sucA and sucB subunits of KGDH as well as the gabD1 and gabD2 subunits of SSADH, explaining the lower label in succinate. There were no changes in the ^{13}C label into histidine and sedoheptulose 7- phosphate (7SP) for antibiotic treated cells indicating that flux through the PPP was not perturbed by antibiotic treatment **(S6A)**. The NADPH/NADP+ ratio measurements revealed no significant differences in antibiotic

treated cells (**Fig. 7D and 7E)**. Overall, there were no changes of flux into the PPP and glyoxylate shunt during our antibiotic assay.

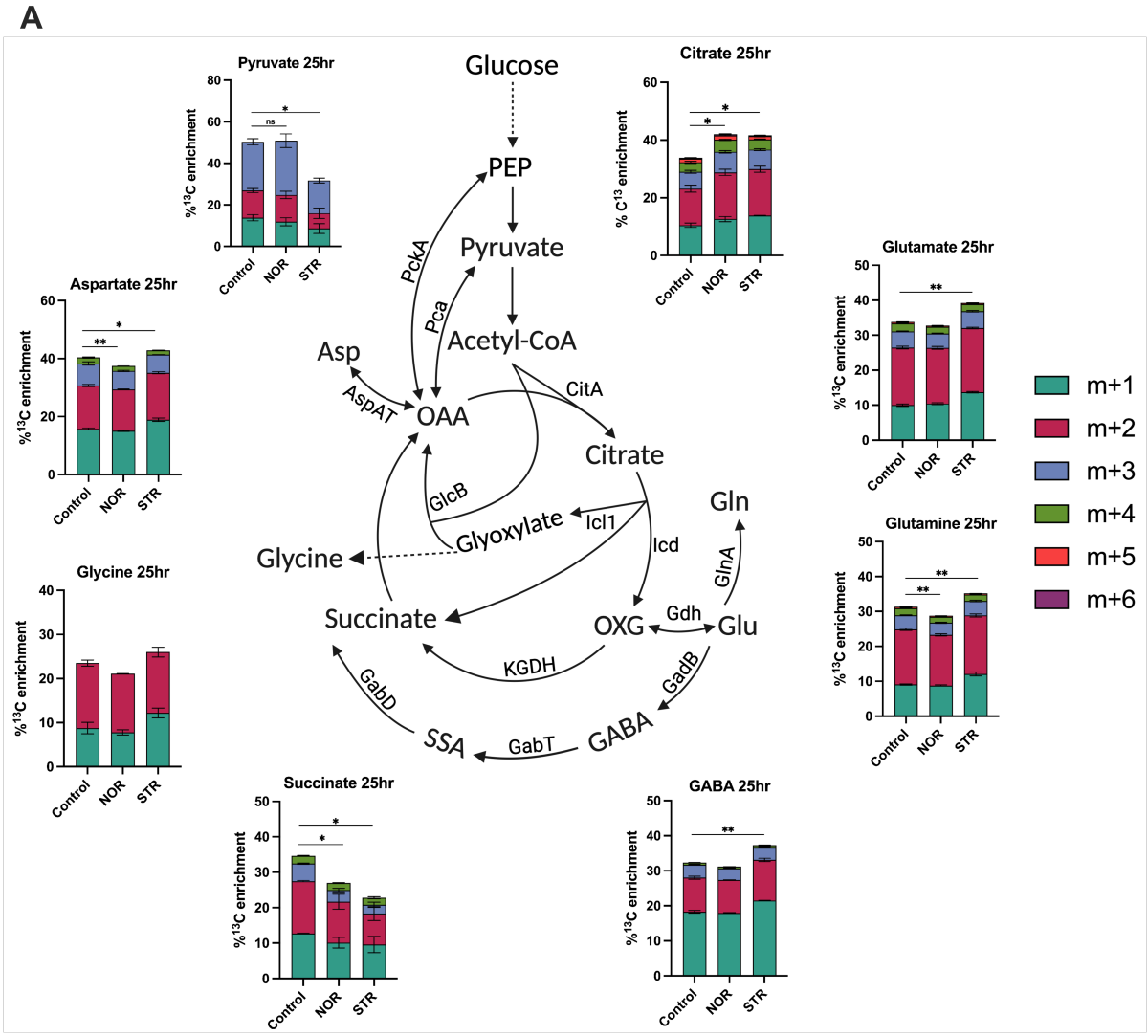
A
Glucose
PEP
Pyruvate
Acetyl-CoA
PckA
Pca
Asp
AspAT
OAA
CitA
Citrate
GlcB
Glyoxylate
Icl1
Icd
Gln
GlnA
Glycine
Succinate
OXG
Gdh
Glu
KGDH
GadB
GabD
SSA
GabT
GABA
Pyruvate 25hr
Citrate 25hr
Aspartate 25hr
Glutamate 25hr
Glycine 25hr
Glutamine 25hr
Succinate 25hr
GABA 25hr
% 13C enrichment
Control
NOR
STR
m+1
m+2
m+3
m+4
m+5
m+6

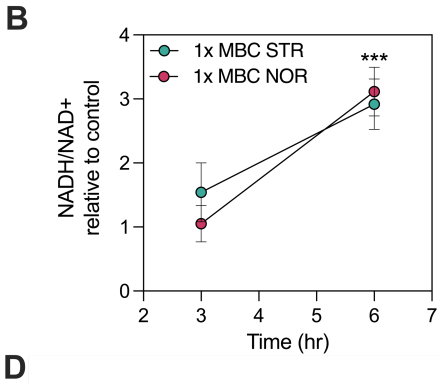
B
1x MBC STR
1x MBC NOR
***
NADH/NAD+ relative to control
Time (hr)

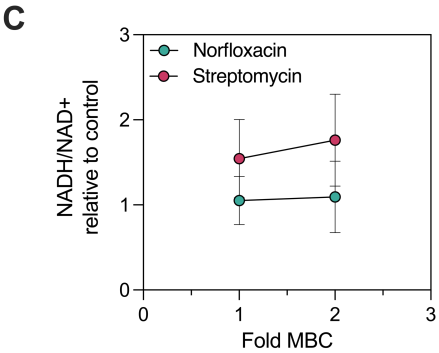
C
Norfloxacin
Streptomycin
NADH/NAD+ relative to control
Fold MBC

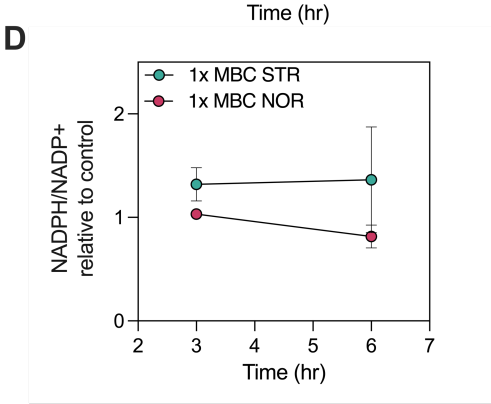
D
1x MBC STR
1x MBC NOR
NADPH/NADP+ relative to control
Time (hr)

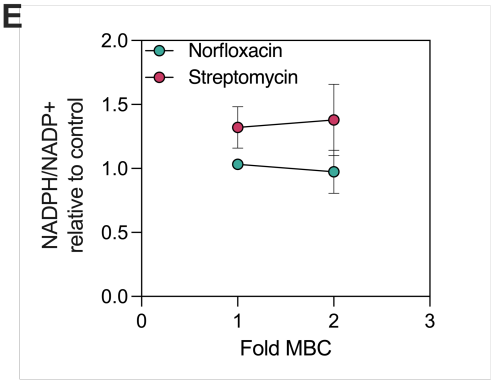
E
Norfloxacin
Streptomycin
NADPH/NADP+ relative to control
Fold MBC

Fig. 7. ^{13}C metabolomics suggests increased metabolic flexibility and bifurcation of TCA cycle flux as bacterial adaptive mechanism

(A) Percent ^{13}C enrichment in CCM metabolites of *M. smegmatis* challenged with ¼x MBC_{99} of norfloxacin and streptomycin at 25 hour time point (recovery phase). "M" denotes the molecular mass of the metabolites, where M+(n) denotes the incorporation of labeled carbon in the metabolites, leading to increase in the mass by that extent. Data for each isotopologue are represented as mean ± SD from independent triplicates. PEP, phosphoenolpyruvate carboxykinase; OXG, alpha-ketoglutarate; Glu, glutamate, Gln, glutamine, OAA, oxaloacetate; Asp, aspartate; GABA, γ-Aminobutyric acid, SSA, succinic semialdehyde. Line graphs represent the ratios of NADH/NAD+ with time (B) and dose-dependent manner (C) for NOR and STR treatments. Figures depict the ratios of NADPH/NADP+ in time (D) and dose-dependent manner (E). Data points represent the mean of at least three independent replicates ± SD. *$p < 0.05$, **$p < 0.01$, ***$p < 0.001$ were calculated by student's t-test (unpaired).

Sub-lethal antibiotic exposure can potentiate development of tolerance and genetic resistance to antibiotics

Next, we questioned whether sublethal antibiotic concentrations have activated any intrinsic drug resistance mechanisms. Specifically, proteomics data analysis revealed a 50-fold upregulation of the protein Eis at 25 hours after STR treatment **(Fig. 8A)**. Eis is known to acetylate and inactivate aminoglycosides, thus conferring antibiotic tolerance and resistance(14,27). This data provides evidence that bacteria may induce intrinsic defence mechanisms to adapt to sub-lethal antibiotic concentrations and that could lead to resistance.

To test the hypothesis that sub-lethal antibiotic concentrations increase mutation frequency, we performed a classical Luria-Delbruck fluctuation test. We harvested cells during the recovery phase (25th hour) and compared the number of rifampicin-resistant bacteria in drug-treated versus untreated conditions. Within 22.5 hours of antibiotic exposure, the mutation frequency of cells adapted to sub-lethal concentrations of streptomycin increased by 4-fold, whereas norfloxacin treatment did not significantly increase the mutational frequency **(Fig. 8B)**. These findings indicate that antibiotic-induced physiological adaptation may facilitate the acquisition of drug-specific mutations or non-specific mutations in metabolic enzymes, leading to antibiotic resistance and treatment failure.

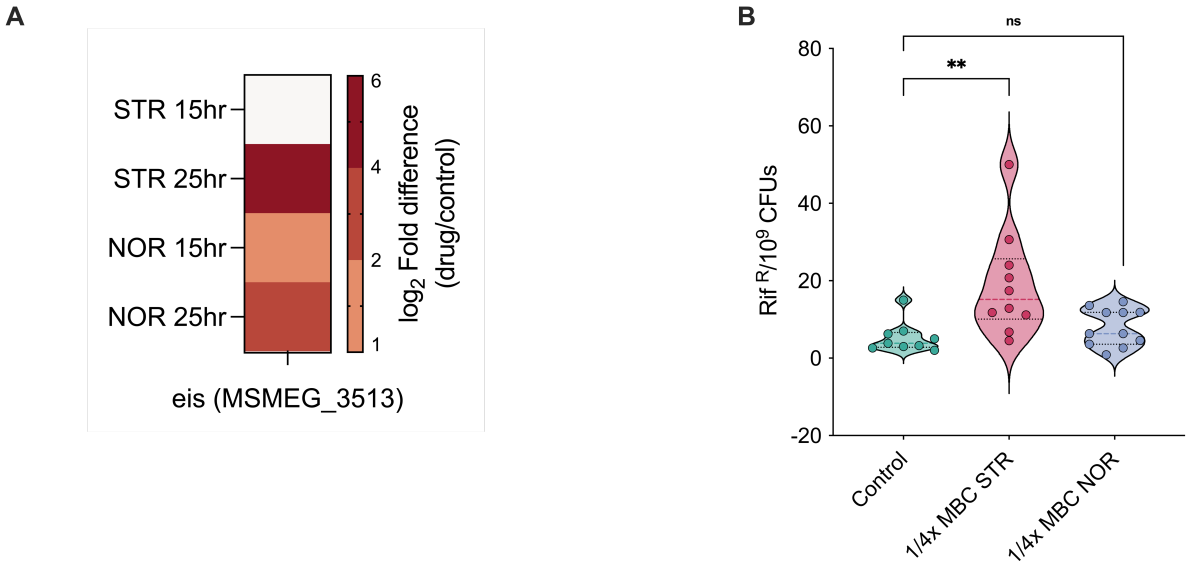

Fig. 8. Sub-lethal antibiotic exposure can potentiate development of antibiotic resistance

Heat map (A) depicting the $\log_2$ fold differences of protein Eis in response to NOR and STR treatment. Figure (B) depicts the mutational frequency of *M. smegmatis* grown in 1/4x MBC_{99} concentrations of norfloxacin and streptomycin for 25 hours; each dot represents the mutational frequency of one replicate.

Discussion:

In conclusion, our model for exploring the mycobacterial responses to antibiotics has determined that an ATP burst is the dominant mechanism driving antibiotic induced cell death. In response to antibiotics, our quantitative proteomics experiments revealed changes in central carbon metabolism and an upregulation of the anti-oxidant response presumably due to the production of reactive oxygen species (ROS). The production of ROS is a proposed universal mechanism that bactericidal antibiotics use to kill bacteria, irrespective of their primary targets(2). These findings led to studies demonstrating that inducing ROS production by increasing respiration with Vitamin C, N-acetylcysteine (NAC), and other thiols enhances antibiotic lethality, including against drug induced-persisters(13,28–30). Similar to our work here, it has been shown that quenching of ROS with various antioxidants protects mycobacteria from antibiotics (25,29,30). Together, ROS has been implicated in antibiotic action and tolerance mechanisms in Gram-positive and Gram-negative bacteria, as well as in mycobacteria.

Despite its widespread appearance and implications, the connection between drug-target interactions and ROS remains unknown. Our measurements revealed increased expression of enzymes involved in central carbon metabolism (CCM), increased flux into the TCA cycle, increased NADH/NAD+ ratios, and elevated ROS levels in response to antibiotic treatment. In conclusion, by increasing cellular respiration, antibiotics induce ROS production and thereby enhance their lethality. While electron leakage from the ETC is the primary source of ROS, it is still unclear how antibiotics modulate ETC and induce ROS production. Recent research has demonstrated that antibiotics deplete the purine nucleotide pool, resulting in an increase in purine biosynthesis and hence ATP demand(31,32). This increased ATP demand was shown to result in increased respiration, oxygen consumption, and ROS production, thus contributing to antibiotic lethality(31).

To confirm that increased respiration led to ROS production in our experiments, we directly measured ATP levels, the end product of aerobic respiration. Both norfloxacin and streptomycin treatments resulted in a substantial dose- and time-dependent rise in ATP levels that was inversely proportional to cell survival. Through inhibition of antibiotic-induced ATP burst using the protonophore CCCP, we confirmed that the observed increase in ATP levels was due to an increase in oxidative phosphorylation and was a significant contributor to antibiotic action and cell death.

Growth rate and metabolism have both been shown to influence antibiotic susceptibility(33–35). A previous study determined that the bacterial metabolic state, not the growth rate, is the prime driver of antibiotic lethality (36). Here we show that ATP levels are the primary driver of antibiotic induced death. As CCCP enhances the respiration and ROS production, the

increased cell survival obtained with antibiotics and CCCP co-treatment reveals that the lethality of antibiotics is determined by the intracellular ATP levels rather than the overall metabolic rate or state of the cells. In addition to increased respiration, our proteomics data show that inhibition of ATP-consuming processes, such as central dogma and cell division, could be contributing to this ATP accumulation. Recent studies have observed a correlation between ATP levels, and antibiotic action and persistence mechanisms. Decreased ATP levels have been identified as the mechanism by which *S. aureus* and *E. coli* generates antibiotic-persister populations(37,38). Similarly, the reduction of ATP levels by arsenate substantially increased the drug-tolerant *E. coli* population(38). Interestingly, exogenous supplementation of alanine or glucose was shown to increase the susceptibility of a drug-resistant strain of *E. tarda* by increasing the flux through the TCA cycle and increasing the proton motive force, resulting in increased kanamycin uptake(39). Consequently, it is plausible that respiration or its end product, ATP, may play a direct or an unusual role in antibiotic action. Supporting this hypothesis, antibiotics that act on the cell wall were shown to increase ATP levels in *M. bovis BCG*, which positively correlated with antibiotic lethality(40). Based on these observations, it is logical to reason that the inhibition of oxidative phosphorylation would correlate with a reduction in bactericidal activity of antibiotics. In agreement with this, it has been reported that energy metabolism inhibitors (BDQ, Q203, and CCCP) inhibit the bactericidal activity of isoniazid and moxifloxacin against *M. bovis BCG* and *M. tuberculosis* (41). These observations support our hypothesis that ATP levels have a direct effect on the efficacy of bactericidal drugs, with high levels of ATP leading to cell death.

Since inhibition of either ROS by GSH/BP or ATP burst by CCCP was sufficient to reduce the lethality of norfloxacin and streptomycin, we sought to determine which of the two is the dominant driver of antibiotic lethality. Intriguingly, measurements of ROS in antibiotic-treated and CCCP-protected bacteria revealed elevated ROS levels were insufficient to cause cell death in the absence of ATP burst, indicating that ATP burst is the dominant mechanism driving cell death. Conditions such as hypoxia, stationary phase, nutrient starvation, biofilm(24,42,43) or the artificial reduction of the NADH/NAD+ ratio(29), make mycobacteria less susceptible to antibiotics than actively growing cells, and this phenotype has been attributed to lower levels of ROS. Based on our findings, we hypothesize that these conditions would also have a lesser flux through the ETC (respiration), which, in addition to decreasing ROS levels, would also have lower levels of ATP. Since the metabolic rate, ROS, and ATP burst are all interdependent and interrelated, studying their individual contributions remains challenging but necessary. Even though the primary effects of antibiotics on their targets and secondary deleterious effects of reactive oxygen species (ROS) are certain and inevitable, they are insufficient to cause rapid bacterial death. We show that in the absence of an ATP burst, bacteria can tolerate target inhibition and ROS for a longer duration.

The antibiotic counter responses by mycobacteria included downregulation of central dogma and cell division processes thereby reducing the availability of the target and antibiotic lethality. In addition, the reduction of these energy consuming processes would reduce anabolic demand and help bacteria decrease the metabolic rate, respiration, ROS production and ATP synthesis. The induction of the anti-oxidant response may provide protection against multiple drugs. In addition, we found increased mutation frequency and the induction of Eis in our

antibiotic assay, thus demonstrating that the antibiotic-adapted population may facilitate the selection of drug-resistant mutants (4,5,14,27). ^{13}C isotopomer analysis of the antibiotic recovery phase revealed a rerouting of the TCA cycle to reduce the production of ROS and ATP. The reduction in flux through the oxidative arm of the TCA cycle was facilitated through metabolic bypass from alpha-ketoglutarate to glutamate-glutamine and GABA. These findings could be used to develop antibiotic adjuvants that enhance aerobic respiration(44), to increase ROS and ATP production for rapid killing of bacteria. Our research provides additional justification for designing drug regimens to avoid antibiotics with overlapping (secondary) actions and, consequently, antibiotic adaptation or tolerance mechanisms. Our study advocates for a thorough understanding of the proximate (primary damage of targets) and ultimate causes (secondary consequences of target inhibition such as ROS and ATP burst) of antibiotic lethality, in order to reduce the risk of cross-tolerance, antibiotic resistance(45).

Materials and Methods

Bacterial strains, growth conditions

Mycobacterium smegmatis MC²155 (Msm) strain was grown in Middlebrook 7H9 broth (Difco) supplemented with 2% Glucose, 0.05% Tween-80 at 37-degree incubator at 200 rpm shaking or on Middlebrook 7H10 agar (m7H10) supplemented with 2% glucose. Msm cells were electroporated with Mrx1-roGFP2 biosensor, which constitutively expresses the sensor under *hsp70* promoter and has hygromycin resistance marker. 50 µg/ml of hygromycin was used to cultivate biosensor harbouring bacteria.

Determination of MIC_{99} and MBC_{99}

A secondary culture of Msm was grown till exponential phase (0.6 OD/ml). MIC was determined by incubating Msm cells (OD = 0.0005/ml) with 2-fold serially diluted antibiotic concentrations for 36 hours. Percentage survival was measured by Alamar Blue assay. The drug concentration that inhibited 99% of bacterial growth was termed as MIC_{99}. For the determination of MBC_{99}, Msm cells from the exponential phase were challenged with various drug concentrations and incubated at 37 degrees in a 96 well plate for 24 hours. The drug concentration that killed 99% ($2\log_{10}$ fold killing) of the initial bacterial population was termed as MBC_{99}. For the experiments requiring different initial inoculum, a corresponding MBC_{99} was determined to account for inoculum effect (that can influence the extent or duration of killing).

Growth curve of *M. smegmatis* with sub-lethal concentration of Norfloxacin and Streptomycin

For the growth curve experiment, a tertiary culture of Msm cells was exposed to either 1x-MBC_{99} or ½x-MBC_{99} or ¼x-MBC_{99} concentrations of norfloxacin and streptomycin, individually, with starting inoculum of 0.0025/ml. Cultures were grown at continuous shaking conditions at 37 degrees. Drug were added at 2.5 hour after the start of the growth curve. For the measurement of viability, cells were serially diluted and plated on LB agar at every 2.5 hour for a total of 25 hours. The experiment was repeated at least 6 times for both the antibiotics.

MIC verification

MIC verification was performed and compared between cells grown with and without the ¼x-MBC_{99} concentrations of norfloxacin and streptomycin, individually, for a total of 25 hour. Cells were harvested from 25th hour and seeded into 96 well plate, pre-seeded with 2 fold serially diluted antibiotic concentrations. Percentage survival was plotted using Alamar Blue assay.

Quantitative Proteomics

Reagents: All reagents were purchased from Sigma Merk. Sequencing grade modified trypsin was purchased from Promega. All the MS grade solvents, water, acetonitrile, and formic acid were procured from Fisher chemicals.

Sample preparation: Proteomic analysis was performed as reported previously (46). For proteomics, cells were grown in 5 independent experiments each for drug treated and untreated conditions. Msm cells were harvested from desired time points and conditions at 6000 g at 4 degrees, washed thrice with chilled PBS (pH=7.4). The cell pellets were stored at -80 degrees until further use. Cell pellets were resuspended in 1ml of lysis buffer (PBS + protease cocktail inhibitor + 1mM EDTA) to minimise non-specific protein degradation. Cells were lysed by mechanical shearing in a bead-beater with at least 10 cycles (7m/s for 45 seconds) of lysis. Tubes were kept on ice for 3-4 minutes in-between the cycles. The supernatant of the cell lysate was precipitated using 1:4 v/v of TCA. Protein precipitates were solubilized in 6M urea and subsequently quantified using BCA kit (Sigma). Ten micrograms of the protein samples were reduced with 10mM dithiothreitol (DTT) and alkylated with 37 mM iodoacetamide (IAA). These linearised proteins in 50mM ammonium bicarbonate (pH = 7.8), were digested with a modified MS grade trypsin (Promega; 1:5 enzyme/protein) overnight at 37 °C. The reactions were terminated by the addition of 2 µl of trifluoroacetic acid (TFA) to bring pH < 2.

Peptide de-salting: Tryptic Peptides were desalted using custom-made stage tips employing the Empore^{TM} C-18 disks. Stage-tips were conditioned and equilibrated with 100% acetonitrile and 0.1% formic acid in water, respectively, before sample loading. Peptides were washed with 0.1% formic acid, eluted using 50% acetonitrile in 0.1% formic acid. For LC-MS analysis, the samples were dried in a vacuum centrifuge to remove acetonitrile and resuspended in 0.1% formic acid.

LC-MS analysis: Peptides were analysed through Ultimate 3000 RSLC nano-UPLC system connected with an Orbitrap Elite hybrid mass spectrometer (Thermo Fisher Scientific). Roughly 600 ng of peptides were loaded with automated injections onto a trap column (Acclaim PepMap^{TM} 100, 3 µm particle size, 75 µm × 2 cm) for 4 min, at a flow rate of 5 µl min^{-1} with 0.1 % formic acid. The peptide separation was achieved on C-18 analytical column (PepMap^{TM} RSLC, 2 µm particle size, 100 Å pore size, 75 µm × 50 cm) at 250 nL min^{-1} flow rate, using the following solvents: solvent A, 0.1% formic acid in water; solvent B, 0.1% formic acid in 100% ACN. Both columns were equilibrated for 10 min with solvent A. A sharp gradient from 1% to 5% B in 3 mins was run, followed by a shallow gradient from 5% to 22% B in 135 mins, and to 28% B in additional 20 mins. The analytical column temperature was maintained at 40°C. A stable spray at a voltage of 1.8 kV was generated using the nano spray electron ionization source (Thermo Fisher Scientific). The capillary temperature was

maintained at 275° C for effective nebulization. The masses were measured in the positive mode using the data-dependent acquisition (DDA). MS1 and MS2 spectra were acquired in Orbitrap (60,000 resolution) and in ion trap analyser (rapid scan mode), respectively. For tandem mass spectrometry, twenty most abundant parent ions were sequentially selected from MS1 spectrum (350-2000 m/z) and fragmented by collision-induced dissociation (CID). For MS1, the maximum ion accumulation time was set at 100 ms with a limitation of $1x10^6$ ions, whereas for MS2 spectra, the ion accumulation time limited 50 ms with a target ion limitation set at $5x10^3$ ions. Peptide fragmentation was performed at 35% of normalized collision energy. Dynamic exclusion of 30 seconds was applied with a repeat count of 1 to avoid repeated analysis of the same peptide.

Protein Identification: 10 raw files for each set of samples (five drug-free control and five ¼x -MBC_{99} drug treated samples) were analysed together by Maxquant (version 2.0.3.0) using the reference proteome of *Mycobacterium smegmatis* mc^2155 (https://mycobrowser.epfl.ch/; version v3) through its internal peptide search engine Andromeda(47,48). The following parameters were used for the protein identification: maximum missed cleavages, 2; mass tolerance for first and main search, 20 and 4.5 ppm respectively; mass tolerance for fragment ion, 0.5 Da; variable modifications used were N-terminal acetylation and methionine oxidation; minimum unique peptide required for identification, 1; minimum peptide length 7; max. peptide mass, 4600 Da; PSM and protein identification FDR were fixed at 0.01; dependent peptide and match between run were enabled with a match time window of 0.7 min and alignment window of 20 min.

Relative protein quantification: The maxLFQ algorithm was enabled in Maxquant for the lable-free quantification (LFQ) of all proteins(49). The protein group files generated from Maxquant were subsequently analysed by Persues (Version: 1.6.2.2) (50). Proteins identified as contaminants, from reverse sequence database as well as through modified peptides were removed. LFQ intensities were log transformed (log_2) and grouped in two groups (drug free and drug treated). Pearson correlation was performed on LFQ intensities to check for the reproducibility and correlation among samples. From 5 independent replicates, 3 highly correlating replicates were chosen for differential expression analysis using volcano plot. Proteins with the fold difference of ±2 with p value ≤ 0.05 were considered to be significantly dys-regulated proteins.

Exclusive expression analysis: Proteins having valid LFQ intensities in all 3 replicates of one condition and were completely absent in all the replicates of other condition, were termed as exclusively/specifically expressed in that particular condition. Similarly, proteins that were specifically repressed/absent in one condition over other, were identified. These proteins are of equal importance since they are only expressed or repressed in response to drugs.

Enrichment analysis

Proteins that were up-regulated as well specifically expressed in response to drugs were analysed by ClueGO, a Cytoscape plug in, for the KEGG Pathway enrichment analysis(51). Only pathways that had p value less than 0.05 were processed further. Benjamini-hochberg multiple correction test was applied and the pathways that were still significant ($p \leq 0.05$) were termed as significantly enriched pathways.

Measurement of Oxidative stress (ROS)

Cells expressing Mrx1-roGFP2 biosensor were challenged with drugs and reagents at different concentrations, and fluorescence was measured at 405 nm and 488 nm excitation wavelengths for a single emission at 520 nm. The ratio of fluorescence intensities obtained at 405 nm and 488 nm (405/488 nm) for 20 mM CHP and 100 mM DTT were used to normalise the data. In response to drugs or other reagents, 405/488 nm ratio was monitored either temporally and for end point in BioTek Synergy H1 Plate Reader using a black 96 well plate (Costar). Since the plate reader measurement requires higher number of cells (100 µl of ~0.8 OD/ml), a separate MBC determination assay was performed to determine the MBC for 0.8 OD/ml culture density to account for inoculum effects.

Time kill kinetics

For the Time kill kinetics, cells with 0.1 OD/ml (~2 x 10^7 CFU/ml) were challenged with different antibiotic concentrations (fold MBC) alone or with other co-supplements in 96 well plate at 37 degrees. At regular interval, cells were aliquoted and diluted in 7h9 + 0.05% Tween-80, and plated on LB agar to enumerate CFUs. After 3-4 days, the colonies were counted manually and plotted as CFU/ml over the course of time to exhibit a time-kill curve.

Measurement of ATP, NADH/NAD+, and NADPH/NADP+ ratio

Cells (0.8 OD/ml) were challenged with various fold MBC concentrations (predetermined for OD 0.8/ml) of norfloxacin and streptomycin. The higher inoculum was taken to ensure sufficient viability of cells upon antibiotic treatment for the detection of ATP, NAD+ and NADP+.

Intracellular ATP levels were determined using the BacTiter-Glo Microbial Cell Viability Assay (Promega) as per manufacturer's instructions. For ATP measurement, cells from various conditions and time points were harvested and heat inactivated at 90 degrees for 30 minutes, as performed elsewhere (52). 25 µl of each sample was mixed with the equal volume of a BacTiter-Glo reagent in a white flat-bottom 96 well plate (Corning). Samples were incubated in dark at room temperature for 5 minutes, and bioluminescence was measured in a BioTek Synergy H1 Plate Reader. The emitted luminescence was divided with the number of viable cells determined just before the heat inactivation to express ATP levels per bacterium (RLS/CFU). The CFU normalised luminescence observed for drug free control was set as 1, and RLS/CFUs values obtained for various conditions were plotted relative to the control.

NADH/NAD and NADPH/NADP ratios were measured using the Bioluminescent NAD/NADH-Glo detection kit (Promega) and NADP/NADPH-Glo detection kit (Promega), respectively, as per manufacturer's instructions. Briefly, cells at desired conditions were lysed using 2 cycles of bead beating (7 m/s for 45 sec). The supernatant of lysate was cleared using the centrifugation and processed for the measurement of NAD/P+ or and NADH/PH separately, and the ratio of luminescence for NADH/NAD+ and NADPH/NADP+ were plotted. The ratios obtained for controls were set as 1, and the ratios obtained for various conditions were plotted with respect to control.

Measurement of respiration using Resazurin

Measurement of metabolic/respiratory activity was performed as reported elsewhere(14). Briefly, cells were grown till exponential phase in 7h9, and treated with desired drugs and

supplements. At indicated time points, 100 µl aliquots of cells were removed and seeded in a black wall 96 well plate (Costar). Resazurin was added to all wells at a final concentration of 30 µg/ml and incubated in dark at 37 degrees for 30 minutes. The quick conversion of resazurin to resorufin was measured in a BioTek Synergy H1 Plate Reader at the excitation of 530 nm and the fluorescence emission of 590 nm. Fluorescence intensities were divided with CFUs, measured just before the addition of the resazurin to express respiratory activity per bacterium. CFU normalised fluorescence intensities acquired for control were set as 1 and CFU normalised intensities obtained for various conditions were plotted relative to the control. The ability of resazurin to differentiate cells with distinct metabolic activity was separately confirmed by comparing normalised fluorescence acquired for cells from exponential phase, stationery phase, PBS starved cells and heat killed cells.

Fluctuation test

Luria-Delbruck fluctuation test was performed to determine if the treatment with the sub-lethal (¼x-MBC_{99} concentrations of norfloxacin and streptomycin, individually) antibiotics increases mutation frequency of cells. 10 ml of exponentially growing cultures of Msm were treated with and without ¼x-MBC_{99} concentrations of norfloxacin and streptomycin for a total of 25 hour at shaking. At 25th hour, 50 µl of cells were serially diluted and plated on LB agar to count CFU/ml, and the rest of the cultures were harvested at 6000 g and resuspended in 300µl of 7h9 + 0.05% Tween-80. 300 µl of suspension was plated onto 2 LB agar supplemented with 100 µg/ml (5x-MIC of RIF on agar) of Rifampicin. Plates were incubated in dark for 4-5 days at 37 degrees, and colonies were counted. The colonies appeared on LB-RIF plates were RIF resisters (Rif^r). Mutation frequency was calculated by dividing the number of RIF resisters with the total number of CFUs plated on LB-RIF plate, and compared between control and drug treatment.

^{13}C isotopologue analysis

Metabolite extraction: The metabolites were extracted and analysed as described elsewhere(53). Briefly, Msm cells were grown till exponential phase (0.6 OD/ml) and diluted to the inoculum of 0.0025 OD/ml in 7h9 supplemented with 0.05% Tween-80, 1% w/v $^{12}C_6$-Glucose and 1% w/v U-$^{13}C_6$ Glucose (50% labelled glucose). Identical to the growth curve and proteomics experiments, antibiotics were added at 2.5 hours and cells were grown with and without ¼x-MBC_{99} concentrations of norfloxacin and streptomycin for a total of 25 hours with shaking. At 25th hour, cells at were harvested and washed twice using chilled PBS at 4000 rpm for 10 minutes. Cells were subsequently resuspended in a pre-chilled methanol:acetonitrile:water (2:2:1), and metabolites were extracted by mechanical lysis with 0.1 mm zirconia beads using FastPrep system (MP Bio) set at 2 cycles of bead beating at 6.5 m/s for 20 seconds. Lysate was spun at 14,000 rpm for 2 minutes in refrigerated centrifuge. The supernatant was filtered using a 0.2 µM cellulose acetate filters, and stored at -80 degrees until further use.

LC-MS analysis: The metabolites were separated using the Agilent InfinityLab Poroshell 120 HILIC-Z (2.1 × 100 mm, 2.7 µm (p/n 675775-924)) column, suitable for polar acidic metabolites. Chromatographic separation was performed using the mobile phase A (10 mM

ammonium acetate in water at pH = 9) and mobile phase B (1.0 mM ammonium acetate at pH = 9) in 10:90 (v:v) water/acetonitrile. Both the solvents were supplemented with a 5 µM Agilent InfinityLab deactivator additive (p/n 5191-4506). The gradient used for the separation is as follows; flow rate of 0.5 ml/min: 0 min, 100% B; 0 to 11.5 min, 70% B; 11.5 to 15 min, 100% B; 12 to 15 min, 100% B; and 5-min of re-equilibration at 100% B. Accurate mass measurements were performed by the Agilent Accurate Mass 6545 QTOF apparatus, connected in line with an Agilent 1290 Infinity II UHPLC. The mass measurement was performed in a negative-ion mode using the following parameters; capillary voltage, 3000 V; fragmentor voltage, 115 V, in centroid 4 GHz mode. The instrument offered mass measurement at less than 5 ppm error with a mass resolution ranging from 10,000 to 45,000 over the fixed m/z range of 121 to 955 atomic mass units. Metabolites were identified based on their accurate masses and their accompanying isotopes. The percent ^{13}C labelling of each metabolite was determined by dividing the summed peak height ion intensities of all ^{13}C-labeled species by the total ion intensity of both labeled and unlabeled ionic species using the Agilent Profinder version B.8.0.00 service pack 3.

Statistical analysis: All the experiments were performed independently at least thrice or more. All the data are represented as the mean and error bars represent the standard deviation. All statistical analysis was performed in Graphpad Prism 9. For the calculation of statistical significance, student's t-test (unpaired, two tailed) for performed in a pair wise manner (between control and the desired experiment).

Acknowledgements:

We thank Prof. John Mackinney for providing us with the gene deletion mutants of *M. smegmatis*. We thank Dr. Areejit Samal for insightful discussions. The authors thank Prof. Amit Singh for a kind gift of the Mrx1-roGFP2 biosensor. The authors thank Annesha Adhikari and Rohit Satardekar for assistance in the experiments. The authors thank Akanksha Agrawal for assistance with creating images. TL thanks CSIR, India for the doctoral research fellowship and the EMBO short-term scientific exchange fellowship. RM thanks DBT, Govt of India for the research grant (BT/PR20820/MED/30/1875/2017). DB thanks Biotechnology and Biological Sciences Research Council (BBSRC) (BB/T007648/1) for research funding.

Competing interests: The authors declare that they have no conflict of interest.

References:

1. Tagliabue A, Rappuoli R. Changing Priorities in Vaccinology: Antibiotic Resistance Moving to the Top. Front Immunol [Internet]. 2018 May 30 [cited 2023 Aug 24];9(MAY):1068. Available from: /pmc/articles/PMC5992407/

2. Kohanski MA, Dwyer DJ, Hayete B, Lawrence CA, Collins JJ. A common mechanism of cellular death induced by bactericidal antibiotics. Cell [Internet]. 2007 Sep 7 [cited 2023 Aug 24];130(5):797–810. Available from: https://pubmed.ncbi.nlm.nih.gov/17803904/

3. Lobritz MA, Belenky P, Porter CBM, Gutierrez A, Yang JH, Schwarz EG, et al. Antibiotic efficacy is linked to bacterial cellular respiration. Proc Natl Acad Sci U S A [Internet]. 2015 Jul 7 [cited 2023 Aug 24];112(27):8173–80. Available from: https://www.pnas.org/doi/abs/10.1073/pnas.1509743112

4. Kohanski MA, DePristo MA, Collins JJ. Sublethal Antibiotic Treatment Leads to Multidrug Resistance via Radical-Induced Mutagenesis. Mol Cell. 2010 Feb 12;37(3):311–20.

5. Levin-Reisman I, Ronin I, Gefen O, Braniss I, Shoresh N, Balaban NQ. Antibiotic tolerance facilitates the evolution of resistance. Science [Internet]. 2017 Feb 24 [cited 2023 Aug 24];355(6327):826–30. Available from: https://pubmed.ncbi.nlm.nih.gov/28183996/

6. Global Tuberculosis Report 2022 [Internet]. [cited 2023 Aug 24]. Available from: https://www.who.int/teams/global-tuberculosis-programme/tb-reports/global-tuberculosis-report-2022

7. Moreno-Gámez S, Kiviet DJ, Vulin C, Schlegel S, Schlegel K, Doorn GS Van, et al. Wide lag time distributions break a trade-off between reproduction and survival in bacteria. Proc Natl Acad Sci U S A [Internet]. 2020 Aug 4 [cited 2023 Aug 16];117(31):18729–36. Available from: https://www.pnas.org/doi/abs/10.1073/pnas.2003331117

8. Dwyer DJ, Belenky PA, Yang JH, Cody MacDonald I, Martell JD, Takahashi N, et al. Antibiotics induce redox-related physi. Proc Natl Acad Sci U S A [Internet]. 2014 May 20 [cited 2023 Aug 24];111(20):E2100–9. Available from: https://www.pnas.org/doi/abs/10.1073/pnas.1401876111

9. Bhaskar A, Chawla M, Mehta M, Parikh P, Chandra P, Bhave D, et al. Reengineering Redox Sensitive GFP to Measure Mycothiol Redox Potential of Mycobacterium tuberculosis during Infection. PLoS Pathog [Internet]. 2014 Jan [cited 2023 Aug 24];10(1):e1003902. Available from: https://journals.plos.org/plospathogens/article?id=10.1371/journal.ppat.1003902

10. Saito K, Mishra S, Warrier T, Cicchetti N, Mi J, Weber E, et al. Oxidative damage and delayed replication allow viable Mycobacterium tuberculosis to go undetected. Sci Transl Med [Internet]. 2021 Nov 24 [cited 2023 Aug 24];13(621):2612. Available from: https://www.science.org/doi/10.1126/scitranslmed.abg2612

11. Saito K, Mishra S, Warrier T, Cicchetti N, Mi J, Weber E, et al. Oxidative damage and delayed replication allow viable Mycobacterium tuberculosis to go undetected [Internet]. Vol. 13, Sci. Transl. Med. 2021. Available from: https://www.science.org

12. Balaban NQ, Helaine S, Lewis K, Ackermann M, Aldridge B, Andersson DI, et al. Definitions and guidelines for research on antibiotic persistence. Nature Reviews Microbiology 2019 17:7 [Internet]. 2019 Apr 12 [cited 2023 Aug 29];17(7):441–8. Available from: https://www.nature.com/articles/s41579-019-0196-3

13. Vilchèze C, Hartman T, Weinrick B, Jacobs WR. Mycobacterium tuberculosis is extraordinarily sensitive to killing by a vitamin C-induced Fenton reaction. Nat Commun [Internet]. 2013 [cited 2023 Aug 27];4. Available from: https://pubmed.ncbi.nlm.nih.gov/23695675/

14. Schrader SM, Botella H, Jansen R, Ehrt S, Rhee K, Nathan C, et al. Multiform antimicrobial resistance from a metabolic mutation. Sci Adv [Internet]. 2021 Aug 1 [cited 2023 Aug 24];7(35). Available from: https://www.science.org/doi/10.1126/sciadv.abh2037

15. Lobritz MA, Belenky P, Porter CBM, Gutierrez A, Yang JH, Schwarz EG, et al. Antibiotic efficacy is linked to bacterial cellular respiration. Proc Natl Acad Sci U S A [Internet]. 2015 Jul 7 [cited 2023 Aug 16];112(27):8173–80. Available from: https://www.pnas.org/doi/abs/10.1073/pnas.1509743112

16. Machová I, Snášel J, Zimmermann M, Laubitz D, Plocinski P, Oehlmann W, et al. Mycobacterium tuberculosis Phosphoenolpyruvate Carboxykinase Is Regulated by Redox

Mechanisms and Interaction with Thioredoxin. J Biol Chem [Internet]. 2014 May 5 [cited 2023 Aug 25];289(19):13066. Available from: /pmc/articles/PMC4036320/

17. Borah Slater K, Beyß M, Xu Y, Barber J, Costa C, Newcombe J, et al. One-shot 13 C15 N-metabolic flux analysis for simultaneous quantification of carbon and nitrogen flux. Mol Syst Biol [Internet]. 2023 Mar 9 [cited 2023 Aug 30];19(3). Available from: https://pubmed.ncbi.nlm.nih.gov/36705093/

18. Viljoen AJ, Kirsten CJ, Baker B, Van Helden PD, Wiid IJF. The role of glutamine oxoglutarate aminotransferase and glutamate dehydrogenase in nitrogen metabolism in Mycobacterium bovis BCG. PLoS One. 2013 Dec 19;8(12).

19. Gallant JL, Viljoen AJ, Van Helden PD, Wiid IJF. Glutamate Dehydrogenase Is Required by Mycobacterium bovis BCG for Resistance to Cellular Stress. PLoS One [Internet]. 2016 Jan 1 [cited 2023 Aug 30];11(1). Available from: https://pubmed.ncbi.nlm.nih.gov/26824899/

20. Cao J, Barbosa JM, Singh NK, Locy RD. GABA shunt mediates thermotolerance in Saccharomyces cerevisiae by reducing reactive oxygen production. Yeast [Internet]. 2013 Apr [cited 2023 Aug 30];30(4):129–44. Available from: https://pubmed.ncbi.nlm.nih.gov/23447388/

21. Ramond E, Gesbert G, Rigard M, Dairou J, Dupuis M, Dubail I, et al. Glutamate Utilization Couples Oxidative Stress Defense and the Tricarboxylic Acid Cycle in Francisella Phagosomal Escape. PLoS Pathog [Internet]. 2014 Jan [cited 2023 Aug 30];10(1):e1003893. Available from: https://journals.plos.org/plospathogens/article?id=10.1371/journal.ppat.1003893

22. Jansen RS, Mandyoli L, Hughes R, Wakabayashi S, Pinkham JT, Selbach B, et al. Aspartate aminotransferase Rv3722c governs aspartate-dependent nitrogen metabolism in Mycobacterium tuberculosis. Nature Communications 2020 11:1 [Internet]. 2020 Apr 23 [cited 2023 Aug 25];11(1):1–13. Available from: https://www.nature.com/articles/s41467-020-15876-8

23. Basu P, Sandhu N, Bhatt A, Singh A, Balhana R, Gobe I, et al. The anaplerotic node is essential for the intracellular survival of Mycobacterium tuberculosis. J Biol Chem [Internet]. 2018 Apr 4 [cited 2023 Aug 25];293(15):5695. Available from: /pmc/articles/PMC5900758/

24. Lee JJ, Lee SK, Song N, Nathan TO, Swarts BM, Eum SY, et al. Transient drug-tolerance and permanent drug-resistance rely on the trehalose-catalytic shift in Mycobacterium tuberculosis. Nature Communications 2019 10:1 [Internet]. 2019 Jul 2 [cited 2023 Aug 29];10(1):1–12. Available from: https://www.nature.com/articles/s41467-019-10975-7

25. Nandakumar M, Nathan C, Rhee KY. Isocitrate lyase mediates broad antibiotic tolerance in Mycobacterium tuberculosis. Nature Communications 2014 5:1 [Internet]. 2014 Jun 30 [cited 2023 Aug 25];5(1):1–10. Available from: https://www.nature.com/articles/ncomms5306

26. Mackenzie JS, Lamprecht DA, Asmal R, Adamson JH, Borah K, Beste DJV, et al. Bedaquiline reprograms central metabolism to reveal glycolytic vulnerability in Mycobacterium tuberculosis. Nature Communications 2020 11:1 [Internet]. 2020 Nov 30 [cited 2023 Aug 30];11(1):1–16. Available from: https://www.nature.com/articles/s41467-020-19959-4

27. Zaunbrecher MA, Sikes RD, Metchock B, Shinnick TM, Posey JE. Overexpression of the chromosomally encoded aminoglycoside acetyltransferase eis confers kanamycin resistance in Mycobacterium tuberculosis. Proc Natl Acad Sci U S A [Internet]. 2009 Nov 24 [cited 2023 Aug 29];106(47):20004–9. Available from: https://pubmed.ncbi.nlm.nih.gov/19906990/

28. Vilchèze C, Hartman T, Weinrick B, Jain P, Weisbrod TR, Leung LW, et al. Enhanced respiration prevents drug tolerance and drug resistance in Mycobacterium tuberculosis. Proc Natl Acad Sci U S A [Internet]. 2017 Apr 25 [cited 2023 Aug 27];114(17):4495–500. Available from: https://pubmed.ncbi.nlm.nih.gov/28396391/

29. Shee S, Singh S, Tripathi A, Thakur C, Kumar AT, Das M, et al. Moxifloxacin-Mediated Killing of Mycobacterium tuberculosis Involves Respiratory Downshift, Reductive Stress, and Accumulation of Reactive Oxygen Species. Antimicrob Agents Chemother [Internet]. 2022 Sep 1 [cited 2023 Aug 27];66(9). Available from: https://pubmed.ncbi.nlm.nih.gov/35975988/

30. Grant SS, Kaufmann BB, Chand NS, Haseley N, Hung DT. Eradication of bacterial persisters with antibiotic-generated hydroxyl radicals. Proc Natl Acad Sci U S A [Internet]. 2012 Jul 24 [cited 2023 Aug 27];109(30):12147–52. Available from: https://www.pnas.org/doi/abs/10.1073/pnas.1203735109

31. Lobritz MA, Andrews IW, Braff D, Porter CBM, Gutierrez A, Furuta Y, et al. Increased energy demand from anabolic-catabolic processes drives β-lactam antibiotic lethality. Cell Chem Biol [Internet]. 2022 Feb 17 [cited 2023 Aug 27];29(2):276-286.e4. Available from: https://pubmed.ncbi.nlm.nih.gov/34990601/

32. Yang JH, Wright SN, Hamblin M, McCloskey D, Alcantar MA, Schrübbers L, et al. A White-Box Machine Learning Approach for Revealing Antibiotic Mechanisms of Action. Cell [Internet]. 2019 May 30 [cited 2023 Aug 27];177(6):1649-1661.e9. Available from: https://pubmed.ncbi.nlm.nih.gov/31080069/

33. Lee AJ, Wang S, Meredith HR, Zhuang B, Dai Z, You L. Robust, linear correlations between growth rates and β-lactam-mediated lysis rates. Proc Natl Acad Sci U S A [Internet]. 2018 Apr 17 [cited 2023 Aug 27];115(16):4069–74. Available from: https://www.pnas.org/doi/abs/10.1073/pnas.1719504115

34. Greulich P, Scott M, Evans MR, Allen RJ. Growth-dependent bacterial susceptibility to ribosome-targeting antibiotics. Mol Syst Biol [Internet]. 2015 Mar 1 [cited 2023 Aug 27];11(3):796. Available from: https://onlinelibrary.wiley.com/doi/full/10.15252/msb.20145949

35. Haugan MS, Løbner-Olesen A, Frimodt-Møller N. Comparative activity of ceftriaxone, ciprofloxacin, and gentamicin as a function of bacterial growth rate probed by Escherichia coli chromosome replication in the mouse peritonitis model. Antimicrob Agents Chemother [Internet]. 2019 Feb 1 [cited 2023 Aug 27];63(2). Available from: https://journals.asm.org/doi/10.1128/aac.02133-18

36. Lopatkin AJ, Stokes JM, Zheng EJ, Yang JH, Takahashi MK, You L, et al. Bacterial metabolic state more accurately predicts antibiotic lethality than growth rate. Nature Microbiology 2019 4:12 [Internet]. 2019 Aug 26 [cited 2023 Aug 27];4(12):2109–17. Available from: https://www.nature.com/articles/s41564-019-0536-0

37. Conlon BP, Rowe SE, Gandt AB, Nuxoll AS, Donegan NP, Zalis EA, et al. Persister formation in Staphylococcus aureus is associated with ATP depletion. Nat Microbiol [Internet]. 2016 Apr 18 [cited 2023 Aug 28];1(5). Available from: /pmc/articles/PMC4932909/

38. Shan Y, Gandt AB, Rowe SE, Deisinger JP, Conlon BP, Lewis K. ATP-Dependent Persister Formation in Escherichia coli. mBio [Internet]. 2017 Jan 1 [cited 2023 Aug 28];8(1). Available from: https://pubmed.ncbi.nlm.nih.gov/28174313/

39. Peng B, Su YB, Tian YM, Correspondence XXP. Exogenous Alanine and/or Glucose plus Kanamycin Kills Antibiotic-Resistant Bacteria. 2015 [cited 2023 Aug 28]; Available from: http://dx.doi.org/10.1016/j.cmet.2015.01.008

40. Shetty A, Dick T. Mycobacterial Cell Wall Synthesis Inhibitors Cause Lethal ATP Burst. Front Microbiol [Internet]. 2018 Aug 15 [cited 2023 Aug 28];9(AUG). Available from: https://pubmed.ncbi.nlm.nih.gov/30158918/

41. Lee BS, Kalia NP, Jin XEF, Hasenoehrl EJ, Berney M, Pethe K. Inhibitors of energy metabolism interfere with antibiotic-induced death in mycobacteria. J Biol Chem [Internet]. 2019 Feb 2 [cited 2023 Aug 28];294(6):1936. Available from: /pmc/articles/PMC6369303/

42. Ojha AK, Baughn AD, Sambandan D, Hsu T, Trivelli X, Guerardel Y, et al. Growth of Mycobacterium tuberculosis biofilms containing free mycolic acids and harbouring drug-tolerant bacteria. Mol Microbiol [Internet]. 2008 Jul [cited 2023 Aug 29];69(1):164–74. Available from: https://pubmed.ncbi.nlm.nih.gov/18466296/

43. Samuels AN, Wang ER, Harrison GA, Valenta JC, Stallings CL. Understanding the contribution of metabolism to Mycobacterium tuberculosis drug tolerance. Front Cell Infect Microbiol. 2022 Aug 22;12:958555.

44. Kitzenberg DA, Lee JS, Mills KB, Kim JS, Liu L, Vázquez-Torres A, et al. Adenosine Awakens Metabolism to Enhance Growth-Independent Killing of Tolerant and Persister Bacteria across Multiple Classes of Antibiotics. mBio [Internet]. 2022 Jun 1 [cited 2023 Aug 27];13(3). Available from: https://journals.asm.org/doi/10.1128/mbio.00480-22

45. Baquero F, Levin BR. Proximate and ultimate causes of the bactericidal action of antibiotics. Nature Reviews Microbiology 2020 19:2 [Internet]. 2020 Oct 6 [cited 2023 Aug 29];19(2):123–32. Available from: https://www.nature.com/articles/s41579-020-00443-1

46. Edna George 1 AG 1, TL 2, PP 1, SI 1, IG 1, LS 1, SJ 1, PRS 1, AAD 1, RM 2, RA. Immunomodulatory effect of mycobacterial outer membrane vesicles coated nanoparticles. Biomaterial Advances.

47. Cox J, Mann M. MaxQuant enables high peptide identification rates, individualized p.p.b.-range mass accuracies and proteome-wide protein quantification. Nature Biotechnology 2008 26:12 [Internet]. 2008 Nov 30 [cited 2023 Aug 30];26(12):1367–72. Available from: https://www.nature.com/articles/nbt.1511

48. Tyanova S, Temu T, Cox J. The MaxQuant computational platform for mass spectrometry-based shotgun proteomics. Nature Protocols 2016 11:12 [Internet]. 2016 Oct 27 [cited 2023 Aug 30];11(12):2301–19. Available from: https://www.nature.com/articles/nprot.2016.136

49. Cox J. Accurate proteome-wide label-free quantification by delayed normalization and maximal peptide ratio extraction, termed MaxLFQ. Mol Cell Proteomics. 2014;13:2513–26.

50. Tyanova S, Temu T, Sinitcyn P, Carlson A, Hein MY, Geiger T, et al. The Perseus computational platform for comprehensive analysis of (prote)omics data. Nature Methods 2016 13:9 [Internet]. 2016 Jun 27 [cited 2023 Aug 30];13(9):731–40. Available from: https://www.nature.com/articles/nmeth.3901

51. Bindea G, Mlecnik B, Hackl H, Charoentong P, Tosolini M, Kirilovsky A, et al. ClueGO: a Cytoscape plug-in to decipher functionally grouped gene ontology and pathway annotation networks. Bioinformatics [Internet]. 2009 Apr 4 [cited 2023 Aug 30];25(8):1091. Available from: /pmc/articles/PMC2666812/

52. Gengenbacher M, Rao SPS, Pethe K, Dick T. Nutrient-starved, non-replicating Mycobacterium tuberculosis requires respiration, ATP synthase and isocitrate lyase for maintenance of ATP homeostasis and viability. [cited 2023 Sep 3]; Available from: http://mic.sgmjournals.org

53. Thomson M, Liu Y, Nunta K, Cheyne A, Fernandes N, Williams R, et al. Expression of a novel mycobacterial phosphodiesterase successfully lowers cAMP levels resulting in reduced tolerance to cell wall–targeting antimicrobials. Journal of Biological Chemistry [Internet]. 2022 Aug 1 [cited 2023 Aug 23];298(8). Available from: http://www.jbc.org/article/S0021925822005932/fulltext